



Application of nanoindentation to evaluate the hardness and yield strength of brass joints produced by FSW: microstructural and strengthening mechanisms

A. Heidarzadeh¹ · M. Paidar² · G. Gülerüz³ · R. Vatankhah Barenji³

Received: 17 February 2020 / Revised: 23 February 2020 / Accepted: 21 March 2020 / Published online: 29 March 2020
© Wrocław University of Science and Technology 2020

Abstract

Nanoindentation test was employed to measure the actual hardness and yield strength of the stir zone in the friction stir-welded single-phase brass joints. For this aim, different joints were prepared according to an experimental matrix based on the central composite rotatable design. In this design matrix, the tool rotational speed, tool traverse speed, and tool axial force were the input parameters. The outputs were the hardness and yield strength of the joints. To measure the hardness and tensile strength of the joints, the nanoindentation test was employed. Moreover, electron back scattered diffraction and transmission electron microscopy techniques were used to study the microstructural features. The results showed that by decreasing rotational speed and axial force, and by increasing the traverse speed, the hardness and yield strength of the joints were increased. In other words, lower heat inputs caused higher strength in the joints. Finer grain sizes, larger grain average misorientation amounts, i.e., existence of more dislocations, and greater Taylor factors in the lower heat input joints revealed that the influence of grain boundaries, dislocations, and texture were the origins of better mechanical properties.

Keywords Friction stir welding · Nanoindentation · OIM · TEM

1 Introduction

The problems associated with conventional fusion welding processes have stimulated researchers to develop new methods for joining materials, particularly difficult-to-join ones [1]. For example, fusion welding processes cause defects arisen from melting and solidification steps including segregations, dendritic structures, porosities, shrinkage, distortions, inclusions, etc. [2]. In this regard, solid-state processes can be good alternatives for fusion welding processes such as arc welding methods. Among all the solid-state processes, friction stir welding (FSW) has attracted a wide interest of researchers [3]. Formation of recrystallized and deformed

microstructures after FSW results in better mechanical properties such as hardness, strength, and ductility [4]. This is since during FSW, the restoration mechanisms such as dynamic recrystallization (DRX) result in finer grain sizes compared to that of the base material (BM) [5].

In recent years, FSW of copper and its alloys (specially the CuZn or brass alloys) has been investigated by researchers [6–16]. For example, Heidarzadeh et al. [6] have compared the FSW of single and double phase brass alloys. They reported that the presence of secondary phase in the double phase brass causes higher strength and lower elongation. Wang et al. [7] have used water flowing during FSW of Cu-30%wt. Zn, which caused formation of grains inside the SZ of the joints with an average size smaller than 1 μm . In addition, they showed that by using water cooling during FSW, the mechanical properties of the joints could be improved considerably. Heidarzadeh et al. [8] have correlated between FSW parameters, grain size, and hardness of friction stir-welded Cu–Zn alloy. They have found that there is deviation from the classical Hall–Petch relationship due to formation of high density of dislocations inside the dynamically recrystallized grains. Mironov et al. [9] have investigated the grain structure formation during FSW of Cu-30%wt. Zn alloy.

✉ A. Heidarzadeh
ak.hz62@gmail.com; ac.heydarzadeh@azaruniv.ac.ir

¹ Department of Materials Engineering, Azarbaijan Shahid Madani University, Tabriz, Iran

² Department of Materials Engineering, South Tehran Branch, Islamic Azad University, Tehran 1459853849, Iran

³ Department of Industrial Engineering, Hacettepe University, 06800 Ankara, Turkey

They demonstrated that the new grains form by bulging of the grain boundaries and nucleation mechanism during FSW, which causes finer grain sizes and high strengths in the joints. Heidarzadeh et al. [10] characterized the final microstructure of the friction stir-welded single-phase brass alloy (70%Cu-30%Zn). They reported that continuous dynamic recrystallization (CDRX) and discontinuous dynamic recrystallization (DDRX) were the main mechanisms of the grain structure formation during FSW. Most recently, Liu et al. [11] have studied the microstructural evolution during FSW of a single-phase brass. They have shown discontinuous dynamic recrystallization (DDRX) in conjunction with annealing twinning is the grain structure formation during FSW. Liu et al. [12] have evaluated the strain and strain rate during rapid cooling friction stir welding of pure copper. Their results showed that the strain in the shoulder-affected zone increases in a two stair-step shape as the material flows from the front to the rear of the tool, corresponding to the first accelerated and then decelerated flow stages. Liu et al. [13], by employing a quasi in situ method, investigated the dynamic evolution of the grain structure considering the flow, strain, and strain rate in the FSW of pure copper. Xu et al. [14] investigated the influence of the Zener–Hollomon (Z) parameter on the microstructure and mechanical properties of copper subjected to FSW. They have suggested that the influence of the post-annealing effect should not be neglected when analyzing the relationship between the Z parameter, microstructure, and mechanical properties. In another investigation, Liu et al. [15] have studied the strain rate-dependent micro-texture evolution in friction stir welding of copper. They found that at different strain rates, different shear texture components form during FSW. Heidarzadeh et al. [16] have studied the effect of stacking fault energy (SFE) on the microstructural evolution during FSW of copper alloys. They confirmed that SFE changes the restoration mechanisms during FSW of copper alloys.

Measuring the actual and accurate mechanical properties of the friction stir-welded joints is challenging using conventional methods due to the following reasons. During FSW, different microstructural zones, including BM, heat affected zone (HAZ), thermomechanically affected zone (TMAZ), and stir zone (SZ), are formed due to a sharp slope of strain, strain rate, and temperature from BM to SZ. The tensile test specimens contain all of the mentioned zones. Thus, the resulted tensile properties cannot be the actual properties of

the SZ [17]. In the case of microhardness, the indentation size effect (ISE) and friction between indenter and material are the main reasons for the inadequate measurements [18]. This fact does not deny the previous reports on the mechanical properties of the friction stir-welded joints. However, to measure the mechanical features of the BM, HAZ, TMAZ, and SZ, the classical tensile test will not be useful.

According to the above literature, a study into the nano-mechanical behavior of friction stir-welded copper alloys is lacking. Therefore, in this study, the nanoindentation has been used to evaluate the nanomechanical properties such as nanohardness and yield strength of the friction stir-welded brass joints.

2 Materials and methods

The BMs used in this study was the single-phase brass (Cu-37 wt.% Zn) sheets with dimensions of 200 mm (length), 100 mm (width), and 2 mm (thickness). The central composite rotatable design was used for the design of experiments, and then the different joints were friction stir-welded at different conditions according to the designed matrix shown in Table 2. It is notable that one joint was produced per condition as shown in Table 2. The FSW tool was made of WC–Co, which had a pin of $\phi 3 \times 1.75$ mm and a shoulder with a diameter of 12 mm. A load-controlled machine was used for FSW. Nanoindentation test was employed in the cross-section of the joints for conducting at least 20 indentations for SZs of the joints by applying the maximum load of 40 mN. For this aim, a MTS XP nanoindenter equipped with a Berkovich diamond indenter was used. The hardness and yielding strength (σ_y) of the SZs were extracted from the nanoindentation data according to the method developed by Dao et al. [19]. Response surface method (RSM) and analysis of variance (ANOVA) were used to evaluate the effect of FSW parameters, including the tool rotational speed (A), tool traverse speed (B), and tool axial force (c), on the mechanical properties. The details of RSM and ANOVA are well explained in the literature [20, 21] and for the sake of brevity are not elucidated in this paper. The design matrix is illustrated in Table 1, which is based on a central composite rotatable design (CCRD). The low-level (−1) and high-level (+1) values were considered

Table 1 Coded and actual values of FSW parameters

Parameters	Unit	Levels				
		−1.68	−1	0	+1	+1.68
Rotational speed (A)	rpm	563	700	900	1100	1236
Traverse speed (B)	mm/min	33	50	75	100	117
Axial force (C)	kN	1.16	1.5	2	2.5	2.8

Fig. 1 The schematic showing the position of specimens for metallography examination and nanohardness analysis

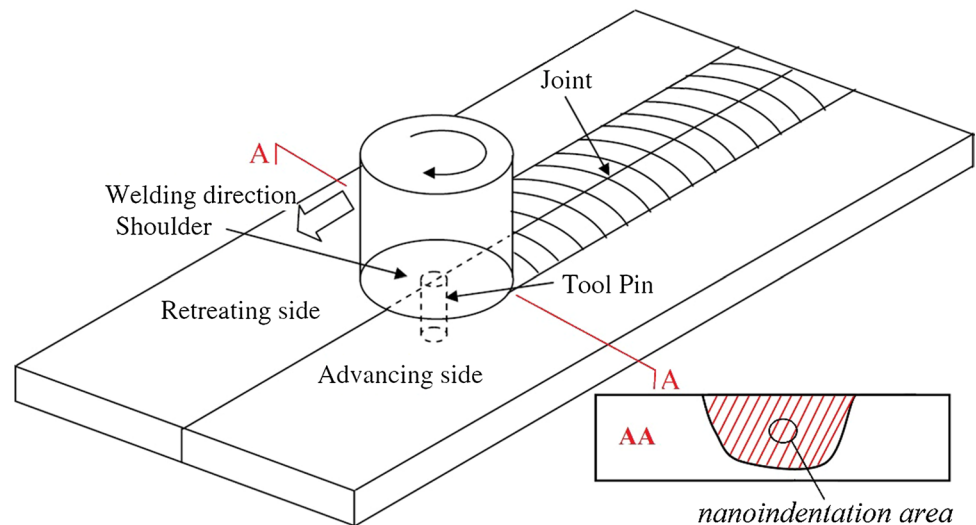


Table 2 Design of experiments. A, B, and C stand for tool rotational speed, tool traverse speed, and tool axial force, respectively

No.	Parameters			Hardness (GPa)			Yield strength (MPa)		
	(A)	(B)	(C)	Exp.	Pred.	Error %	Exp.	Pred.	Error %
1	700	50	1.5	2.89±0.22	2.89	0	154±5.21	153	0.6
2	1100	50	1.5	2.25±0.08	2.32	-3.1	124±3.51	125	-0.8
3	700	100	1.5	3.29±0.12	3.26	0.9	172±1.14	170	1.2
4	1100	100	1.5	2.8±0.31	2.77	1.1	150±3.06	145	3.3
5	700	50	2.5	2.75±0.21	2.73	0.7	138±5.01	138	0
6	1100	50	2.5	2.74±0.18	2.71	1.1	132±6.11	129	2.3
7	700	100	2.5	2.65±0.14	2.52	4.9	153±4.03	147	3.9
8	1100	100	2.5	2.64±0.19	2.58	2.3	145±4.32	141	2.8
9	564	75	2.0	3.02±0.23	3.09	-2.3	164±2.17	167	-1.8
10	1236	75	2.0	2.65±0.07	2.66	-0.4	135±1.81	139	-3
11	900	33	2.0	2.67±0.15	2.63	1.5	129±3.64	128	0.8
12	900	117	2.0	2.71±0.22	2.83	-4.4	143±2.22	151	-5.6
13	900	75	1.2	2.78±0.24	2.74	1.4	146±4.60	148	-1.4
14	900	75	2.8	2.34±0.16	2.46	-5.1	127±3.19	133	-4.7
15	900	75	2.0	2.82±0.17	2.82	0	151±3.81	152	-0.7
16	900	75	2.0	2.8±0.17	2.82	-0.7	152±3.76	152	0
17	900	75	2.0	2.81±0.16	2.82	-0.4	153±4.41	152	0.7
18	900	75	2.0	2.83±0.17	2.82	0.4	152±3.76	152	0
19	900	75	2.0	2.83±0.17	2.82	0.4	152±3.76	152	0
20	900	75	2.0	2.83±0.16	2.82	0.4	152±3.76	152	0

according to the literature and our experiences to produce sound welds. The microstructure of the joints was first examined by using an optical microscopy (OM). The OM specimens were cross-sectioned from the joints perpendicular to the FSW direction, and they were then prepared by mechanical polishing and etching with a solution of 50 mL HCl, 10 mL H₂O and 5 g FeCl₃. A Philips XL30 E-SEM field emission gun scanning electron microscope equipped with electron backscattered diffraction (EBSD) system was employed for OIM. The average grain size of

the samples was calculated by OIM software according to ASTM standard. The specimens for OIM were finalized after mechanical polishing by electropolishing for 30 s in a solution containing 250 mL H₃PO₄, 250 mL ethanol, 50 mL propanol, 500 mL distilled water, and 3 g urea at 10 V and 25 °C. Transmission electron microscopy (TEM, JEOL JEM 2010) was used for more clarification of the microstructural details. For TEM sample preparation, the electrojet thinning was used with a solution of 30% H₃PO₄ and 70% distilled water at the applied potential of 80 V.

The position of specimens for metallography examination and nanohardness analysis is illustrated in Fig. 1, schematically.

3 Results and discussion

In Table 2, the experimental and predicted results for the hardness and σ_y are listed for the different joints. Besides, the actual versus predicted values for both the hardness and σ_y are plotted in Fig. 2.

According to Table 2, the errors are between $\pm 5\%$, which confirms the plots in Fig. 2 because the actual and predicted responses have lied on a line with a slope of 45° . Thus, the predicted values are very close to experimental values. Furthermore, the ANOVA data (Table 3) showed that the R^2 value for both hardness and σ_y were higher than 95%. Therefore, the developed models were adequate to evaluate the effect of parameters. The perturbation plots for hardness and σ_y are illustrated in Fig. 3, which indicate how the parameters influence the responses. In perturbation plots, a response is plotted versus an input parameter when the other parameters are set constant at their zero level. The established relationships were as follows:

$$\begin{aligned} \text{Hardness (GPa)} = & +2.82 - 0.13A + 0.06B - 0.88C \\ & + 0.019AB + 0.14AC - 0.14BC \\ & + 0.021A^2 - 0.031B^2 - 0.083C^2 \end{aligned} \quad (1)$$

Table 3 ANOVA data for the hardness and yield strength

Response	R^2	Adj R^2	Mean	Standard deviation
Hardness (GPa)	0.92	0.86	2.75	0.082
Yield strength (MPa)	0.92	0.84	146.20	4.87

$$\text{Yield strength (MPa)} = +146.20 - 8.41A + 7.00B - 4.76C \quad (2)$$

As can be seen from Eqs. 1 and 2, quadratic and linear models were significant for the hardness and yield strength, respectively. This is why, in the perturbation plots (Fig. 3), hardness curves show nonlinear behavior and yield strength shows linear behavior.

According to Fig. 3, rotational speed and axial force have a similar effect on the hardness and σ_y . By increasing the rotational speed and axial force, both the hardness and σ_y decrease, continuously. On the other hand, tool traverse speed had a different effect in a way that by increasing it, the responses increase, continuously. The origin of this effect will be cleared in the next paragraphs by comparison between two joints welded at different FSW conditions.

All of the 20 joints welded at different conditions (Table 2) showed typical and same macrostructures. For example, the macrostructure and microstructures of different areas of the joint welded at condition of experiment number 5 are shown in Fig. 4. As shown in Fig. 4, the joints composed of different microstructural zones of BM, TMAZ,

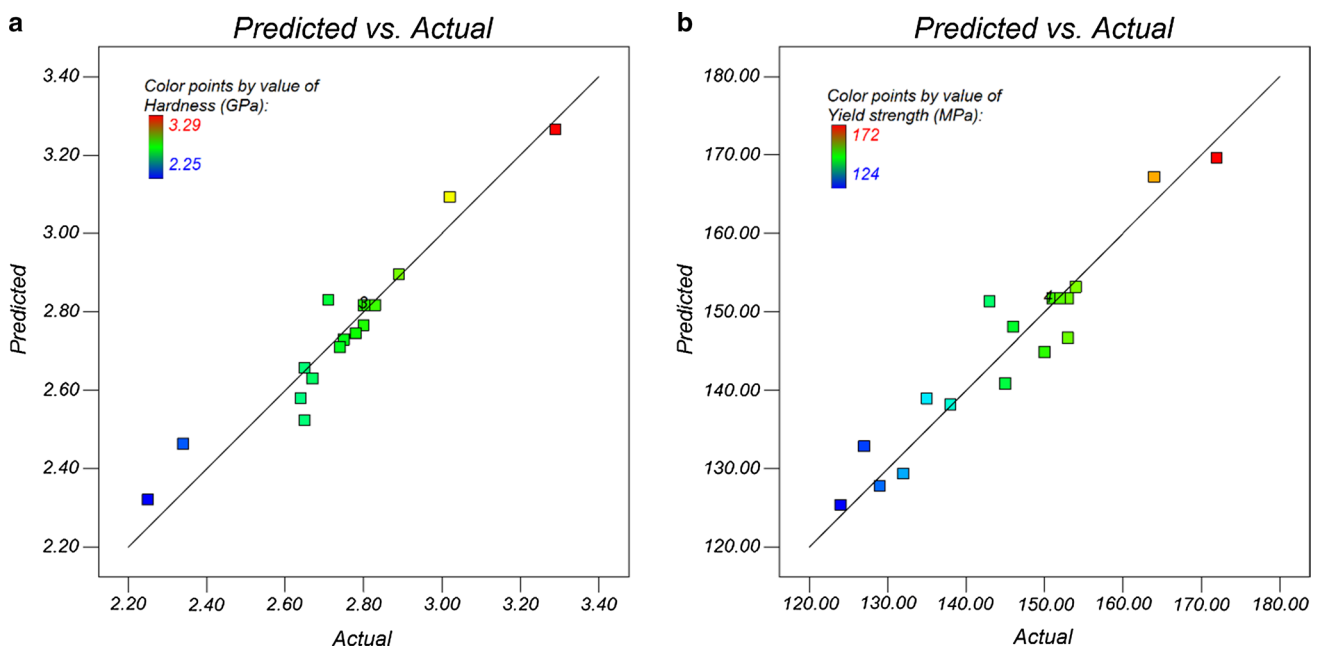


Fig. 2 Actual versus predicted plots of the joints: **a** hardness, and **b** yield strength

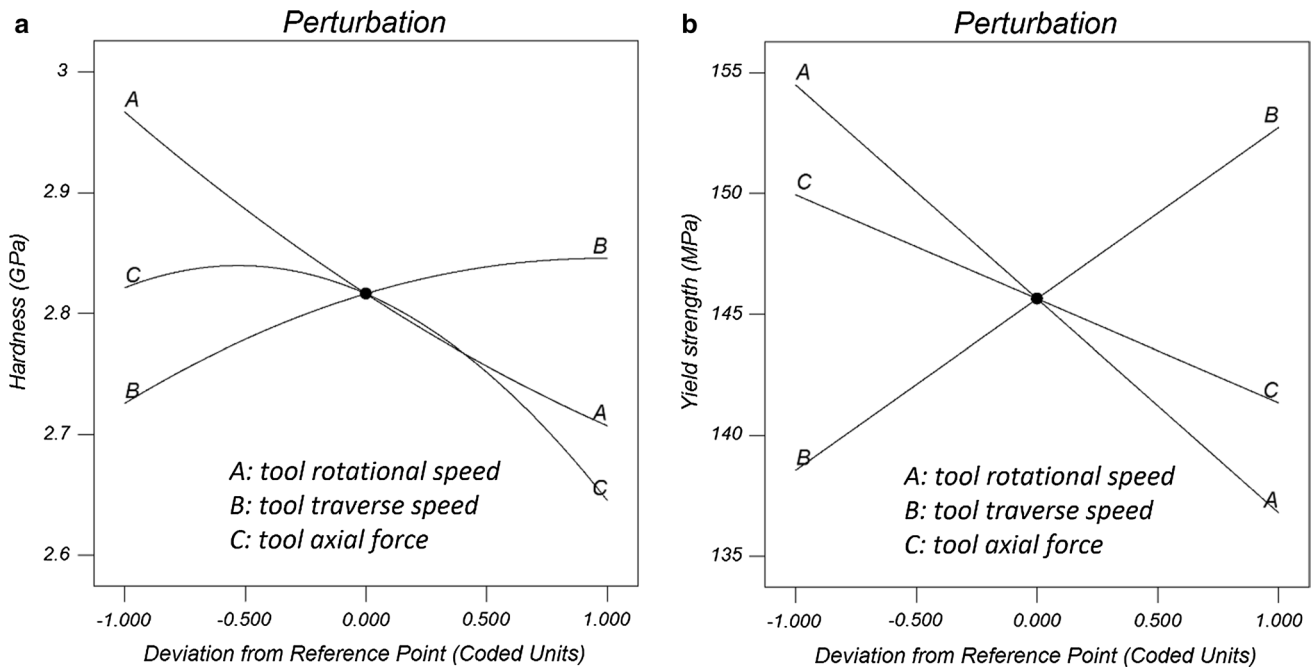


Fig. 3 Perturbation plots showing the effect of the FSW parameters on the mechanical properties of the joints: a hardness, and b yield strength

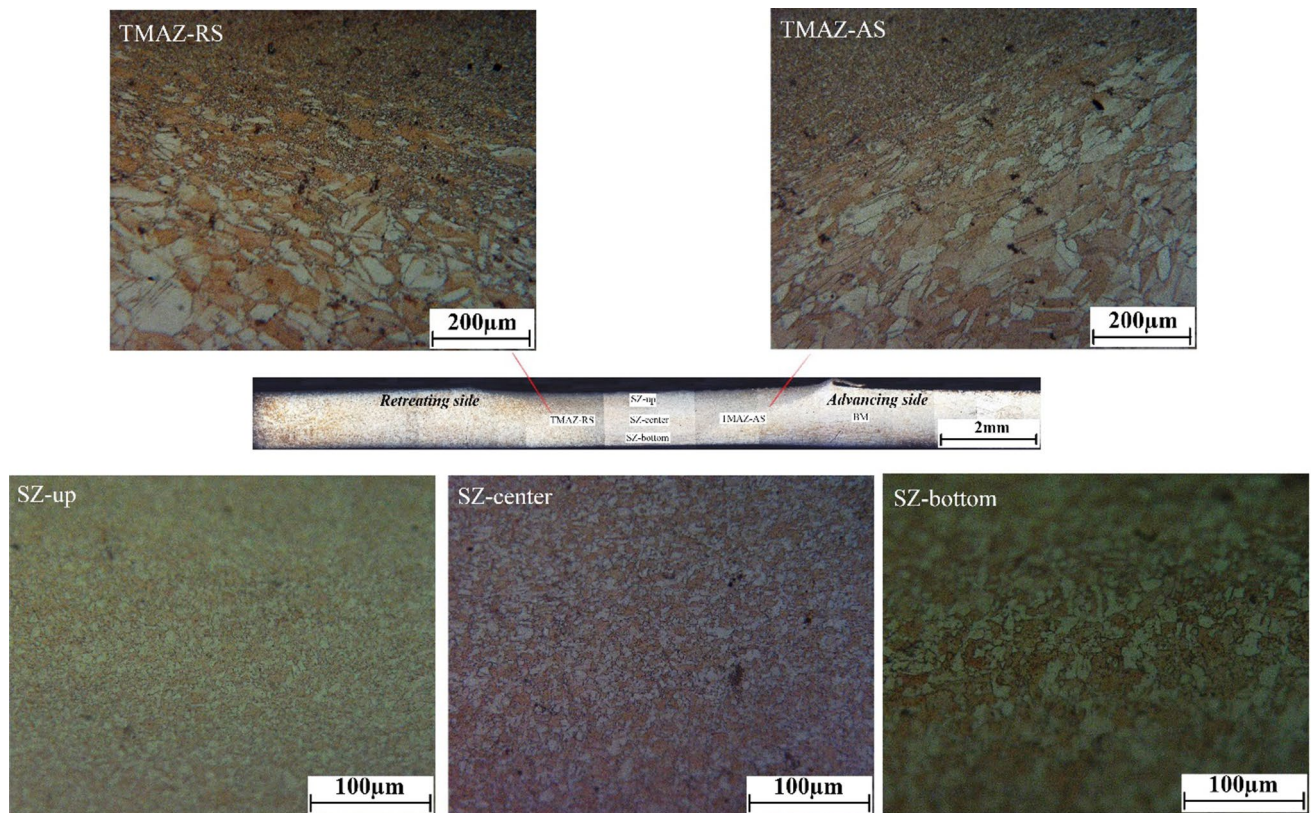


Fig. 4 The macrostructure and microstructures of different areas in the joint welded at condition of experiment number 5

and SZ. The HAZ was not seen in all joints, which is due to high thermal conductivity of the brass plates. In addition, it can be found that the grain size in SZ is not uniform, and it decreases from bottom to up side of the SZ, which is due to larger strain and strain rates underneath the shoulder area. The nanoindentation and microstructural investigations have been conducted on SZ-center area indicated in Fig. 4.

To compare between the joints welded at low and high heat input conditions, joints number 3 and 18 (Table 2) were selected, and their microstructures were characterized using OIM and TEM. The nanoindentation curves and

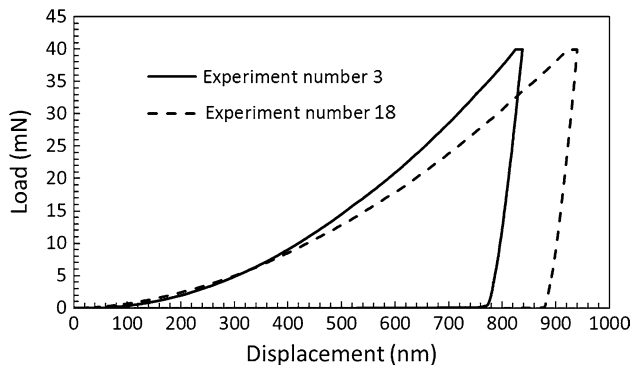


Fig. 5 Load–displacement plot for the joints welded at different conditions

OIM data of these joints are shown in Figs. 5 and 6. The OIM results include inverse pole figure (IPF), grain average misorientation (GAM), and Taylor factor maps. In addition, the quantitative OIM data are illustrated in Figs. 7, 8 and 9. From Figs. 6 and 7, the joints number 3 and 18 have an average grain size of 7.3 μm and 15.4 μm , respectively. A comparison between the grain size of BM (31.6 μm) and the joints indicates that FSW leads to grain refinement. During FSW due to the presence of heat and deformation, dynamic restoration mechanisms such as dynamic recrystallization generate the new fine grains inside the SZs [16, 22–26]. Recently, it is demonstrated that both the continuous and discontinuous dynamic recrystallization (CDRX and DDRX) occur during FSW of brasses [9, 10, 27]. It is believed that with increasing the Zn content in brasses and using lower heat inputs during FSW, the DDRX fraction increases during grain structure formation [16, 24]. In this study, due to higher rotational speed and lower traverse speed, the joint number 3 (rotational speed of 700 rpm and traverse speed of 100 mm/min) has a lower heat input condition compared to that of the joint number 18 (rotational speed of 900 rpm and traverse speed of 75 mm/min). It is well documented that stir zone temperature or heat input is a direct function of rotational speed. In addition, traverse speed has an inverse effect on heat input [28, 29]. Thus, according to the same chemical composition for the joints (37 wt.% Zn), the lower heat

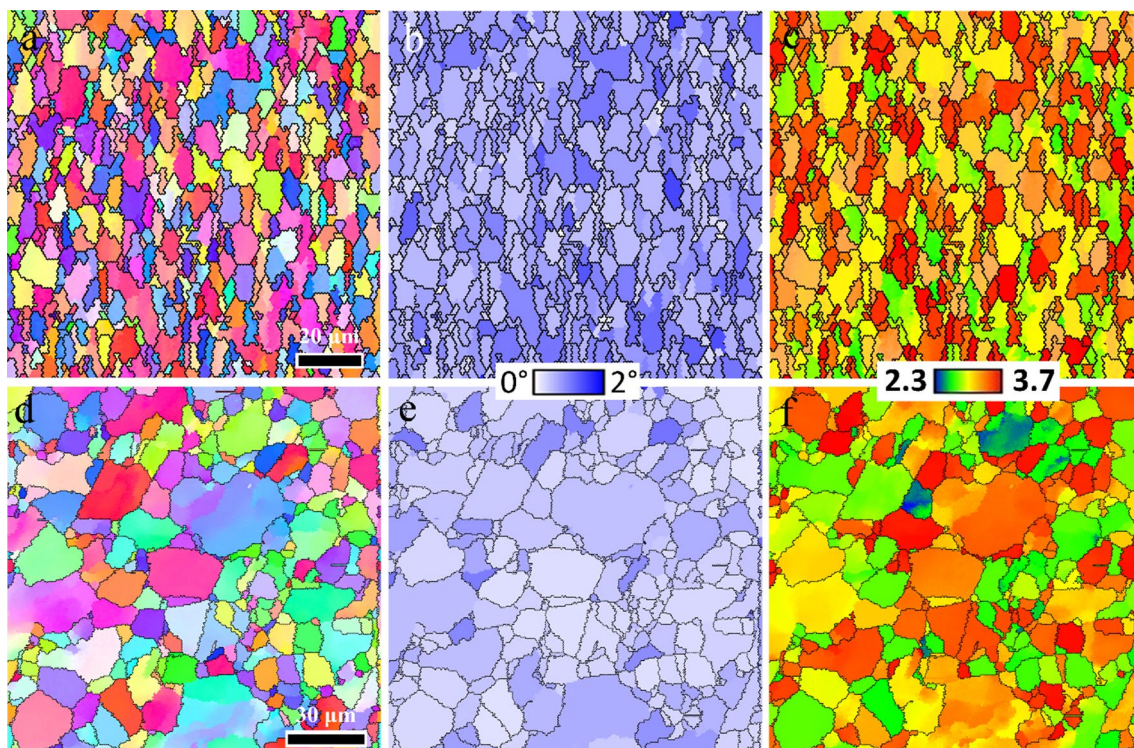


Fig. 6 The OIM data including IPF, GAM, and Taylor factor, respectively, for the joints welded at different conditions: (a–c) experiment number 3 with an average grain size of 7.3 μm , and (d–f) experiment number 18 with an average grain size of 15.4 μm

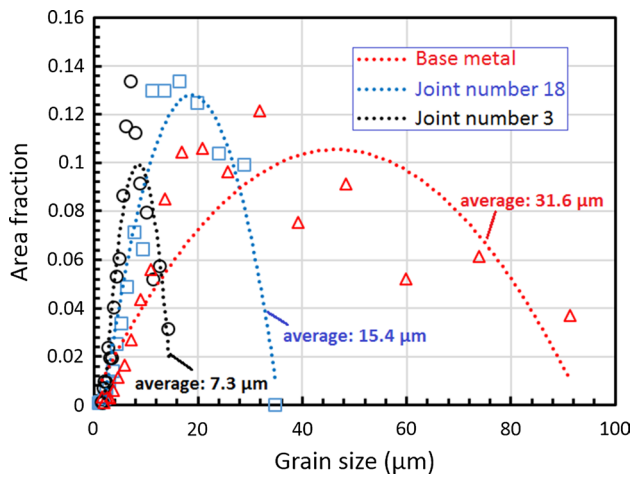


Fig. 7 The grain size distribution of the base metal and joints welded at different conditions

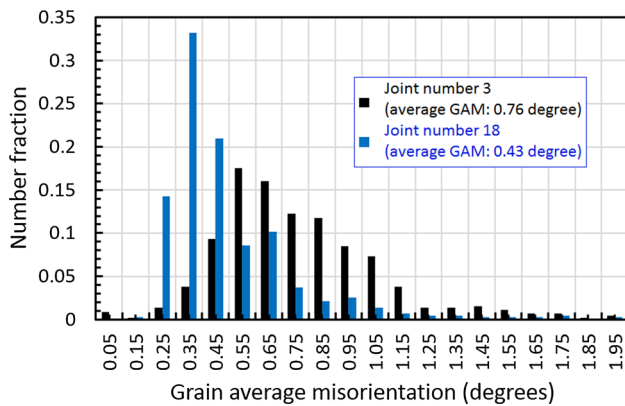


Fig. 8 Grain average misorientation (GAM) distribution of the joints welded at different conditions

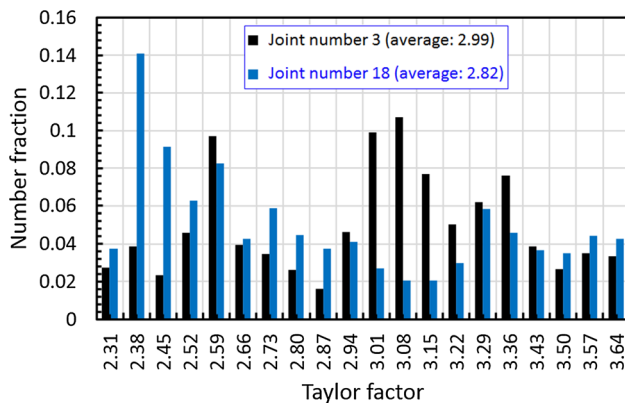


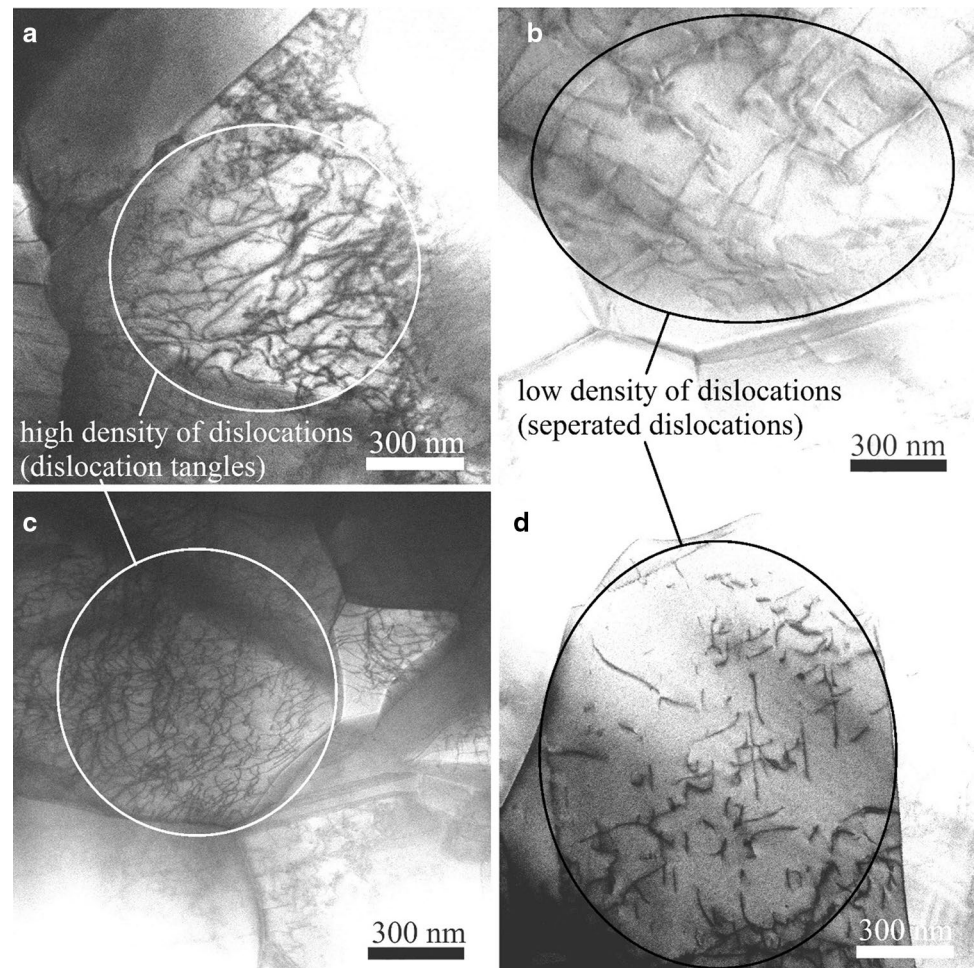
Fig. 9 Taylor factor distribution of the joints welded at different conditions

input condition of the joint number 3 results in more DDRX mechanism, and hence by reduction in grain size from 7.3 to 15.4 μm (i.e., 52.5% reduction), finer grains are formed.

According to Table 2 and Fig. 5 (nanoindentation curves), joint number 3 has higher hardness and σ_y amounts compared to those of the joint number 18. The origin of these different mechanical properties for different heat input conditions can be discussed by strengthening mechanism as follows. (1) Joint number 3 (lower heat input joint) has finer grain sizes compared to joint number 18 (higher heat input joint) according to Figs. 6 and 7. Finer grain sizes mean that the fraction of high angle grain boundaries (HAGBs) is high, which act as an obstacle to the dislocation movement, and hence causes higher strength according to $\Delta\sigma_{gb} = \alpha_2 Gb \left[(1 - f_{Re}) \left(\frac{1}{\delta} \right) + f_{Re} \left(\frac{1}{D} \right) \right]$ relationship [30–33]. In this relationship, $\Delta\sigma_{gb}$ is the amount of increment in yield strength due to HAGBs, α_2 is a constant, G is shear modulus, b refers to Burgers vector, f_{Re} is the proportion of recrystallized part, δ belongs to subgrain size, and D is grain size. The OIM results showed that the fraction of HAGBs for BM, joint number 18, and joint number 3 were equal to 54.1%, 81.5%, and 92.3%, correspondingly. Thus, FSW has caused higher amounts of HAGBs, which can be a sign of DDRX. As well, the formation of more HAGBs in the lower heat inputs in conjunction with finer grain sizes reveals that DDRX mechanism with randomizing texture feature is more probable during FSW. (2) The dislocation density has a direct effect on the strength of the joints according to $\Delta\sigma_D = \alpha_1 Gb \sqrt{\rho}$ equation in which $\Delta\sigma_D$ is the amount of increment in yield strength due to dislocation density (ρ), and α_1 is a constant. Dislocations act as barriers to the movement of each other during mechanical tests. Thus, higher dislocation density causes more barriers [34, 35].

For exploring the dislocation density in the samples, GAM and TEM images have been used. The higher the GAM values, the higher the dislocation densities [36]. Comparison between GAM maps (Fig. 6b, e) and GAM distribution plots (Fig. 8) shows that the joint number 3 has higher dislocation density than that of the joint number 18. This means that using lower heat input during FSW, the final grains of SZ contain more dislocations. The TEM images of the joints number 3 and 18 confirm this conclusion, which is shown in Fig. 10. According to Fig. 10, the joint number 3 contains more dislocations with tangled structure (Fig. 10a, c) than that of the joint number 18 (Fig. 10b, d). (3) The effect of texture on the strength can be stated as the Taylor factor, in which the higher Taylor factor amount causes higher strength value [31]. From Figs. 6c, f, and 9, the joint number 3 has higher Taylor factor than joint number 18. In summary, the strengthening mechanisms of grain

Fig. 10 The TEM images of the joints welded at the condition of the experiment number: (a and c) 3, and (b and d) 18



boundaries, dislocations, and texture effect result in higher strength in the joints welded at lower heat inputs.

4 Conclusions

The nanomechanical properties such as hardness and yield strength of the friction stir welded brass joints have been investigated, and the following conclusions can be summarized. The hardness values in the range of 2.25–3.29 GPa and the yield strength values in the range of 124–172 MPa can be obtained after FSW in the SZ of the joints. Rotational speed and axial force have the same effect on the nanomechanical properties in a way that by decreasing them the hardness and yield strength increase. However, tool traverse speed has the opposite effect. In fact, by changing the FSW parameters, the heat input changes, and hence it affects the governing mechanism during grain structure formation. At lower heat inputs (lower rotational speed, lower axial force, and higher traverse speed), the proportion of DDRX increases. More DDRX causes finer grain sizes, more HAGBs, larger GAM amounts, and larger

Taylor factor. Finer grain sizes and more HAGBs stimulate the strengthening mechanism of grain boundaries because they prohibit the dislocation movement. Larger GAM values reveal that dislocation density is higher than that of the high heat input joints, as confirmed by TEM images, which shows that the other strengthening mechanism is the effect of dislocation density. Moreover, larger Taylor factor, which usually stands for the effect of texture on the strength of the materials, demonstrates that the other active strengthening mechanism is the effect of texture. Consequently, the joints welded at lower heat inputs have higher strength than the joints welded at higher inputs due to strengthening mechanisms of grain boundaries, dislocations, and texture effect.

Acknowledgements The first author expresses his gratefulness to Dr. Roghayeh Mohammadzadeh, the assistant professor of Materials Engineering Department in Azarbaijan Shahid Madani University, for his useful discussion on mechanical properties. This work was supported by Farda-Negar (knowledge-based) Co. Iran, Research and Development project grant number 2019/1112. Authors gratefully appreciate practical support from Mr. Bagher Alashoar, the Chairman of Farda-Negar (knowledge-based) Co.

Data availability The raw/processed data required to reproduce these findings cannot be shared at this time due to legal or ethical reasons.

References

- Çam G. Friction stir welded structural materials: beyond Al-alloys. *Int Mater Rev*. 2011;56(1):1–48.
- Zolghadr P, Akbari M, Asadi P. Formation of thermo-mechanically affected zone in friction stir welding. *Mater Res Express*. 2019;6(8):086558.
- Çam G, İpekoğlu G. Recent developments in joining of aluminum alloys. *Int J Adv Manuf Technol*. 2017;91(5):1851–66.
- Akbari M, Asadi P. Optimization of microstructural and mechanical properties of friction stir welded A356 pipes using Taguchi method. *Mater Res Express*. 2019;6(6):066545.
- Mironov S, Sato YS, Kokawa H. Friction-stir welding and processing of Ti–6Al–4 V titanium alloy: a review. *J Mater Sci Technol*. 2018;34(1):58–72.
- Heidarzadeh A, Saeid T. A comparative study of microstructure and mechanical properties between friction stir welded single and double phase brass alloys. *Mater Sci Eng, A*. 2016;649:349–58.
- Wang YF, An J, Yin K, Wang MS, Li YS, Huang CX. Ultrafine-grained microstructure and improved mechanical behaviors of friction stir welded Cu and Cu–30Zn joints. *Acta Metall Sin (Engl. Lett.)*. 2018;31:878.
- Heidarzadeh A, Saeid T. Correlation between process parameters, grain size and hardness of friction-stir-welded Cu–Zn alloys. *Rare Met*. 2016. <https://doi.org/10.1007/s12598-016-0704-9>.
- Mironov S, Inagaki K, Sato YS, Kokawa H. Development of grain structure during friction-stir welding of Cu–30Zn brass. *Phil Mag*. 2014;94(27):3137–48.
- Heidarzadeh A, Saeid T, Klemm V. Microstructure, texture, and mechanical properties of friction stir welded commercial brass alloy. *Mater Charact*. 2016;119:84–91.
- Liu XC, Sun YF, Nagira T, Ushioda K, Fujii H. Correction to: microstructure evolution of Cu–30Zn during friction stir welding. *J Mater Sci*. 2018;53(15):11130.
- Liu XC, Sun YF, Nagira T, Ushioda K, Fujii H. Experimental evaluation of strain and strain rate during rapid cooling friction stir welding of pure copper. *Sci Technol Weld Join*. 2019;24(4):352–9.
- Liu XC, Sun YF, Nagira T, Ushioda K, Fujii H. Evaluation of dynamic development of grain structure during friction stir welding of pure copper using a quasi in situ method. *J Mater Sci Technol*. 2019;35(7):1412–21.
- Xu N, Feng RN, Guo WF, Song QN, Bao YF. Effect of Zener–Hollomon parameter on microstructure and mechanical properties of copper subjected to friction stir welding. *Acta Metall Sin*. 2019;33:319.
- Liu XC, Sun YF, Nagira T, Ushioda K, Fujii H. Strain rate dependent micro-texture evolution in friction stir welding of copper. *Materialia*. 2019;6:100302.
- Heidarzadeh A, Saeid T, Klemm V, Chabok A, Pei Y. Effect of stacking fault energy on the restoration mechanisms and mechanical properties of friction stir welded copper alloys. *Mater Des*. 2019;162:185–97.
- Charitidis CA, Dragatogiannis DA, Koumoulos EP, Kartsonakis IA. Residual stress and deformation mechanism of friction stir welded aluminum alloys by nanoindentation. *Mater Sci Eng A*. 2012;540:226–34.
- Koumoulos EP, Charitidis CA, Daniolos NM, Pantelis DI. Nano-mechanical properties of friction stir welded AA6082-T6 aluminum alloy. *Mater Sci Eng B*. 2011;176(19):1585–9.
- Dao M, Chollacoop N, Van Vliet KJ, Venkatesh TA, Suresh S. Computational modeling of the forward and reverse problems in instrumented sharp indentation. *Acta Mater*. 2001;49(19):3899–918.
- Barenji RV, Pourasl HH, Khojastehnezhad VM. Electrical discharge machining of the AISI D6 tool steel: prediction and modeling of the material removal rate and tool wear ratio. *Precis Eng*. 2016;45:435–44.
- Eshghi AT, Lee S. Adaptive improved response surface method for reliability-based design optimization. *Eng Opt*. 2019;51:1–19.
- Etter AL, Baudin T, Fredj N, Penelle R. Recrystallization mechanisms in 5251 H14 and 5251 O aluminum friction stir welds. *Mater Sci Eng, A*. 2007;445–446:94–9.
- Heidarzadeh A. Tensile behavior, microstructure, and substructure of the friction stir welded 70/30 brass joints: RSM EBSD, and TEM study. *Arch Civil Mech Eng*. 2019;19(1):137–46.
- Heidarzadeh A, Motalleb-nejad P, Barenji RV, Khalili V, Güteryüz G. The origin of the maximum hardness of the friction stir welded single-phase Cu–Zn plates: RSM EBSD, and TEM investigation. *Mater Chem Phys*. 2019;223:9–15.
- McNalley TR, Swaminathan S, Su JQ. Recrystallization mechanisms during friction stir welding/processing of aluminum alloys. *Scripta Mater*. 2008;58(5):349–54.
- Sun YF, Xu N, Fujii H. The microstructure and mechanical properties of friction stir welded Cu–30Zn brass alloys. *Mater Sci Eng A*. 2014;589:228–34.
- Liu X, Sun Y, Nagira T, Ushioda K, Fujii H. Microstructure evolution of Cu–30Zn during friction stir welding. *J Mater Sci*. 2018;53(14):10423–41.
- Mishra RS, Ma ZY. Friction stir welding and processing. *Mater Sci Eng R Rep*. 2005;50(1):1–78.
- Besharati-Givi M, Asadi P. *Advances in friction stir welding and processing*. Cambridge: Elsevier-Woodhead Publishing; 2014.
- Starink MJ, Deschamps A, Wang SC. The strength of friction stir welded and friction stir processed aluminium alloys. *Scripta Mater*. 2008;58(5):377–82.
- Starink MJ, Wang SC. A model for the yield strength of overaged Al–Zn–Mg–Cu alloys. *Acta Mater*. 2003;51(17):5131–50.
- Benson DJ, Fu H-H, Meyers MA. On the effect of grain size on yield stress: extension into nanocrystalline domain. *Mater Sci Eng A*. 2001;319–321:854–61.
- Schulson EM, Weihs TP, Viens DV, Baker I. The effect of grain size on the yield strength of Ni₃Al. *Acta Metall*. 1985;33(9):1587–91.
- Wang S, Zhu Z, Starink M. Estimation of dislocation densities in cold rolled Al–Mg–Cu–Mn alloys by combination of yield strength data, EBSD and strength models. *J Microsc*. 2005;217(2):174–8.
- Sastry SML. The effect of grain size on yield stress and work hardening in Cu₃Au. *Mater Sci Eng*. 1976;22:237–43.
- Tian YZ, Gao S, Zhao LJ, Lu S, Pippan R, Zhang ZF, Tsuji N. Remarkable transitions of yield behavior and Lüders deformation in pure Cu by changing grain sizes. *Scripta Mater*. 2018;142:88–91.

Publisher's Note Springer Nature remains neutral with regard to jurisdictional claims in published maps and institutional affiliations.